ACS APPLIED MATERIALS & INTERFACES

Research Article

www.acsami.org

Engineering the Mechanical Properties of Polymer Networks with Precise Doping of Primary Defects

Doreen Chan,[†] Yichuan Ding,[‡] Reinhold H. Dauskardt,[‡] and Eric A. Appel*[,‡]

[†]Department of Chemistry and [‡]Department of Materials Science and Engineering, Stanford University, Stanford, California 94305, United States

Supporting Information

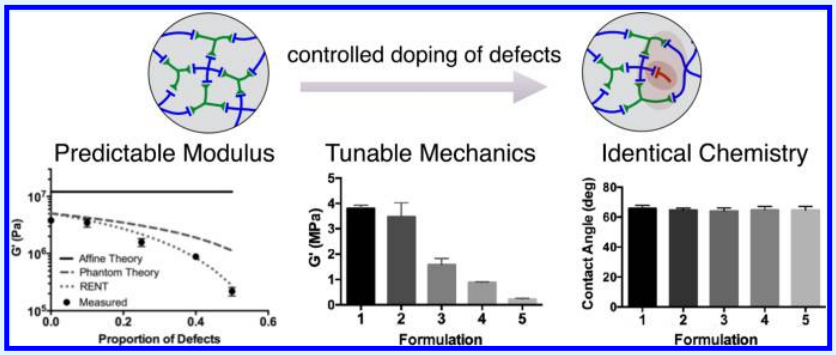

ABSTRACT: Polymer networks are extensively utilized across numerous applications ranging from commodity superabsorbent polymers and coatings to high-performance microelectronics and biomaterials. For many applications, desirable properties are known; however, achieving them has been challenging. Additionally, the accurate prediction of elastic modulus has been a long-standing difficulty owing to the presence of loops. By tuning the prepolymer formulation through precise doping of monomers, specific primary network defects can be programmed into an elastomeric scaffold, without alteration of their resulting chemistry. The addition of these monomers that respond mechanically as primary defects is used both to understand their impact on the resulting mechanical properties of the materials and as a method to engineer the mechanical properties. Indeed, these materials exhibit identical bulk and surface chemistry, yet vastly different mechanical properties. Further, we have adapted the real elastic network theory (RENT) to the case of primary defects in the absence of loops, thus providing new insights into the mechanism for material strength and failure in polymer networks arising from primary network defects, and to accurately predict the elastic modulus of the polymer system. The versatility of the approach we describe and the fundamental knowledge gained from this study can lead to new advancements in the development of novel materials with precisely defined and predictable chemical, physical, and mechanical properties.

KEYWORDS: *polymeric materials, mechanical properties, hydrogels, elastomers, defects*

INTRODUCTION

The prevalence of polymer networks, such as thermosets, gels, and elastomers, can been seen extensively in industrial commodities (e.g., superabsorbents, adhesives, coatings, and composites)[1] as well as in high-performance applications in microelectronics[2−4] and biomedicine.[5−8] Dielectric elastomers have, for example, been exploited for their electromechanical properties in applications ranging from actuators and sensors to artificial muscles.[3,9−11] For many applications, specific mechanical properties are desired, yet are often difficult to obtain and to predict. Typically, these materials are formed through the polymerization of multifunctional monomers that act as cross-linking nodes within the network. These nodes must have a critical average functionality to yield a completely percolated network, and both the density and functionality of these nodes are crucial in dictating specific mechanical, physical, and chemical properties (e.g., degradation,[12] transport and conductivity,[13] and swelling[14−16]) of these materials. To modulate these properties, researchers typically seek to alter the molecular weight of oligomeric or polymeric precursors, the functionality of the cross-linking moieties, or the stoichiometric ratio of multifunctional monomers. Yet, these approaches often lead to changes in network chemistry, which may be useful in some circumstances, but is often detrimental to full exploitation in end-use applications.[17,18] Alternatively, defects can be introduced in the network through dangling chains, which create mechanical inefficiencies to polymeric networks.[19,20] Furthermore, predicting the mechanical properties of polymer networks has been difficult owing to the uncontrolled and unquantified presence of defects such as loops.[21−23] The

Received: September 21, 2017
Accepted: November 14, 2017
Published: November 14, 2017

DOI: 10.1021/acsami.7b14376
ACS Appl. Mater. Interfaces 2017, 9, 42217−42224

development of network disassembly spectroscopy by Johnson et al. to count loops in polymer networks led to the development of the real elastic network theory (RENT) to quantitatively determine the impact of these defects on mechanical properties.[1,21,24]

Mark et al. investigated the effects of dangling chain defects by tuning the cross-linking density in poly(dimethylsiloxane) (PDMS) networks and by examining the resulting mechanical properties.[25,26] Although these studies demonstrated that changing the functionality of the PDMS network results in an increase in dangling chains and a decrease in strength, here we independently tuned the functionality of the polymer network while also controlling the concentration of primary loops to precisely engineer the relationship between primary defects and elasticity while controlling the surface chemistry.

Additionally, it has been challenging to precisely determine the relationship between the molecular structure and mechanical properties of polymer networks owing to the presence of defects in the network, whereby affine and phantom network theories of elasticity do not agree with the experimental values of G' for a large array of systems. The inability of these theories to accurately describe elastic modulus inspired the development of RENT, as reported by Olsen and Johnson,[21] which accounts for the elastic ineffectiveness of loops (e.g., primary, secondary, and higher-ordered loops), as well as the negative impact of these defects on the elastic effectiveness of the network in their vicinity. Although RENT closely models the observed modulus values in gels by precisely describing the mechanical impact of loop-based defects, the degree of looping could not be affected a priori, except by the alteration of component mixing during polymerization.[27,28] Precisely tuning the degree of loop formation has also been of known difficulty. Herein, we synthesize a series of cross-linked elastomers with different stoichiometric ratios of monovalent and trivalent thiol-functional monomers with a four-arm functional alkene monomer, while keeping the total thiol−ene stoichiometry constant, to introduce primary defects into the polymer network. This approach to doping of primary defects provides an opportunity to quantitatively model the impact of these defects on mechanical behavior and allows for the precise tuning of mechanical properties, without alteration of the network molecular formula and critical physical properties. We demonstrate that RENT can be applied to our model system to accurately predict the elastic modulus.

EXPERIMENTAL SECTION

Materials. 3-Mercaptopropionate, trimethylolpropane-tris(3-mercaptopropionate), pentaerythritol allyl ether, and 2,2-dimethoxy-2-phenylacetophenone (DMPA) were purchased from Sigma-Aldrich and used as received.

General Preparation of Elastomers. Prepolymer formulations containing thiol, alkene, and DMPA (1 wt %) were mixed, briefly centrifuged to remove bubbles, loaded between two glass slides separated by a silicone spacer (0.254 mm ± 0.0508 mm), and subsequently polymerized in a Luzchem photoreactor system with 8 W bulbs and an intensity of 25−30 W/m^2 (LZC-4, $h\nu$ = 350 nm, 5 min).

Differential Scanning Calorimetry. Glass transition temperature (T_g) measurements were performed with differential scanning calorimetry (DSC) using a TA Instrument Q2000 calorimeter. Samples were first cooled from room temperature to −90.00 °C and ramped at 10.00 °C/min to 140.00 °C to remove thermal history. The samples were then cooled at 5.00 °C/min to −90.00 °C and ramped at 10.00 °C/min to 140.00 °C. The T_g values were measured from the trace of the second cycle.

Rheological Characterization. Oscillatory rheology measurements were performed with a TA Instruments AR-G2 rheometer. Amplitude sweeps were conducted at a frequency of 10 rad/s from 0.1 to 100%. Frequency sweeps were conducted at 0.1% strain from 0.1 to 100 rad/s. All tests were performed at 25 °C using an 8 mm parallel-plate geometry.

Instron. Samples were cut into dogbone geometries, and tensile strength measurements were performed with an Instron series 5560A with 100 N load cell. Tensile tests were conducted at 0.01 mm/s at room temperature.

Delamination Tests. For the cohesion study, it is important to secure all of the interfaces in the double cantilever beam (DCB) specimens so that the delamination will not occur adhesively at any point of the interface, such that the crack will propagate cohesively. Thus, the method used to bond the samples to the beam support may vary between samples and should have no significant effect on the measured cohesion value, as long as the crack is cohesive within the sample. For the adhesion study, the surface of the beams was identical between samples (glass), and identical surface functionalization was induced on the glass slides to allow for direct comparison between formulations. To perform cohesion tests of **1** and **2**, DCB specimens were prepared by bonding the thin films of elastomers in between two 3 mm thick poly(methyl methacrylate) (PMMA) substrates using a highly cross-linked brittle epoxy (Loctite EA E-20NS). The DCB specimens were then thermally cured for 1.5 h at 80 °C in air. Cohesion tests for polymer Formulation **3** were carried out by the direct polymerization of elastomers between glass slides functionalized with thiols. Surface hydroxyl groups on glass slides were activated by oxygen plasma for 3 min, and slides were then immersed into 2 v/v % (3-mercaptopropyl)trimethoxysilane in dry toluene and incubated overnight. Slides were rinsed with ethanol and dried with nitrogen twice. The elastomer solution was pipetted between thiol-functional slides. Samples for cohesion tests of **4** and **5**, and all samples for adhesion tests were prepared as follows. After a 3 min treatment to oxygen plasma, the glass slides were immersed in a solution of 2 v/v % allyltriethoxysilane and dry toluene overnight. The slides were rinsed with ethanol and dried with nitrogen twice before use. All delamination tests were carried out in the laboratory air environment, which remained constant at 25 °C and approximately 40−45% RH.

Microneedle Fabrication. Prepolymer solutions were pipetted into microneedle molds (ST-10 × 10-H600B200P500, Micropoint Technologies) with 600 μm needle height and 200 μm base. Filled molds were degassed in the dark for 5 h and photocross-linked as described in the above experimental protocols. Samples were carefully peeled out of molds and imaged with a U1 Series SuperSpeed camera (Ramé-Hart).

Contact Angle. Contact angle measurements were performed with dI H_2O (3 μL) using a contact angle goniometer (Ramé-Hart 290).

X-ray Photoelectron Spectroscopy. Disks of elastomer samples were cut and degassed overnight under vacuum and analyzed with a PHI VersaProbe 1 scanning X-ray photoelectron spectroscopy (XPS) microprobe.

Swelling Ratio and Degradation. The elastomers (8 mm punches) were placed in 24-well plates with either dI H_2O pH = 2 or pH = 11. The samples were stored at room temperature in the dark, and the mass of elastomers was taken before and after 9 days.

Optical Properties. UV−vis−NIR spectroscopy was performed with an Agilent Cary Series 6000i, and transmittance was measured from 200 to 1000 nm.

Statistical Analysis. All values of significance were determined using a one-way analysis of variance with Prism GraphPad 6 software. Post hoc comparisons were performed with Tukey's multiple comparison test.

RESULTS AND DISCUSSION

Thiol−ene "click" chemistry is the reaction of thiols with alkenes, typically terminal alkenes, and is particularly useful in the preparation of intricate cross-linked networks on account of insensitivity to water and oxygen[29] and ability to be

DOI: 10.1021/acsami.7b14376
ACS Appl. Mater. Interfaces 2017, 9, 42217−42224

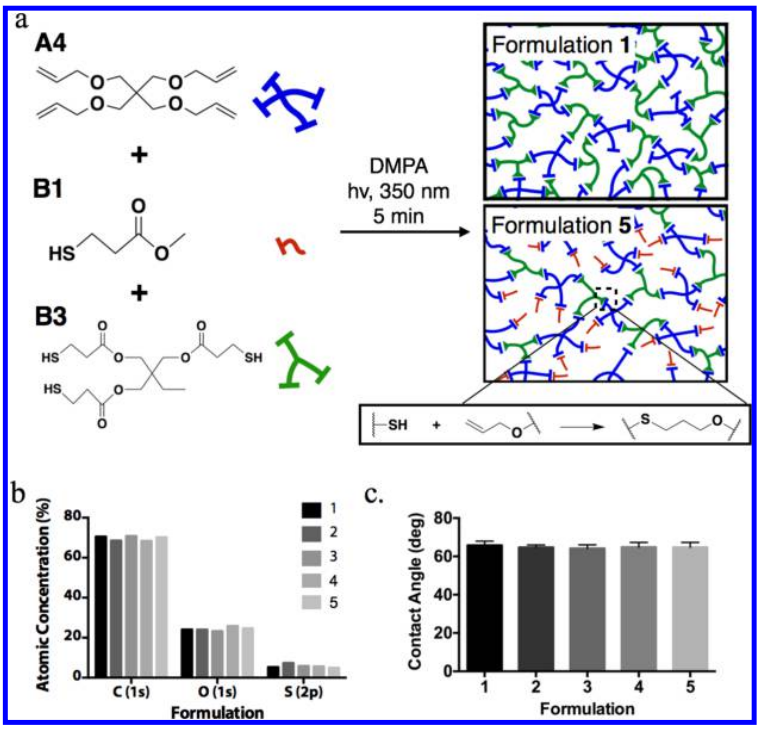

Figure 1. (a) Schematic illustration of the photopolymerization of pentaerythritol allyl ether (**A4**), 3-mercaptopropionate (**B1**), and trimethylolpropane-tris(3-mercaptopropionate) (**B3**) using DMPA as an initiator. By varying the ratio of **B1** and **B3**, while maintaining the overall ratio of thiols to allyl moieties, primary network defects are introduced without alteration of the chemistry of the resulting materials. (b) XPS indicated that the atomic concentrations of carbon, oxygen, and sulfur species are equivalent across all formulations (n.b. accuracy with standardless quantification in XPS is ∼10%). (c) Water contact angle measurements indicated identical hydrophilicity across all formulations (n = 5; data presented as mean ± SD).

photoinitiated.[30−32] Moreover, thiol−ene-based materials have been investigated extensively,[33] which exhibit highly homogeneous networks[34] and negligible volume change upon polymerization.[29,35] The versatility and selective reactivity of this chemistry have notably been used to create microarray cell culture substrates for high-throughput screening applications[36] and substrates for soft imprint lithography.[37] Here, to modulate the mechanical properties of thiol−ene elastomers without altering their molecular formulation, blends of thiol-based monomers comprising one- and three-arm thiols were photopolymerized with a multiarm allyl-functional monomer (Figure 1a). Although others have utilized different model systems, such as the combination of **A4** and **A3** monomers,[28] this system was specifically chosen as a more precise introduction of defects that allows for modeling of the system. Specifically, elastomer formulations were prepared with pentaerythritol allyl ether (**A4**), trimethylolpropane-tris(3-mercaptopropionate) (**B3**), and varying amounts of 3-mercaptopropionate (**B1**), whereby the total concentration of functional thiol and alkene groups remained constant (Table 1). **A4** was added at 5 mol % end group excess to total thiol concentration to facilitate ease of fabrication and handling of materials, as well as to ensure that desired cross-links were driven to completion. The introduction of **B1** effectively creates primary defects within the network (Figure 2e), yielding a simple approach to doping of defects.

Elastomer polymerization was initiated by DMPA (1 wt %) irradiated with UV light (λ = 350 nm) for 5 min to ensure complete photopolymerization (Figure S1). Highly transparent

Table 1. Formulations and Calculated Average Functionality Used Throughout the Study

entry	A4[a]	B1[a]	B3[a]	f_{avg}[b]	T_g (°C)[c]
1	1.05	0.00	1.00	3.44	−13.43
2	1.05	0.10	0.90	3.09	−25.04
3	1.05	0.25	0.75	2.69	−32.56
4	1.05	0.40	0.60	2.38	−42.29
5	1.05	0.50	0.50	2.21	−50.18

[a]Molar equivalence of end-group functionality in the prepolymer formulation. [b]Average functionality, f_{avg}, of each formulation as determined by eq 2. [c]Glass transition temperature as determined by DSC.

materials were formed (Figure S2). Owing to the similarity in the chemical structure of the allyl groups, we expected that the detectable chemical features would be indistinguishable among materials. The elemental composition of samples was examined with XPS (Figure 1b), which indicated no significant variation between samples. The high spectral and depth resolution (5 nm) of XPS indicates that surface functionality is preserved across all formulations. Additionally, contact angle measurements indicated identical hydrophilicity among samples (Figure 1c), further emphasizing the preservation of surface chemical and physical (i.e., roughness) properties among formulations. Further, these polymer networks exhibited no degradation by mass percent over 9 days in acidic (pH 2) and basic (pH 11) aqueous conditions, again verifying the stability of the system (Figure S3). With the current approach, the presence of excess allyl functionality could allow for surface modification

DOI: 10.1021/acsami.7b14376
ACS Appl. Mater. Interfaces 2017, 9, 42217−42224

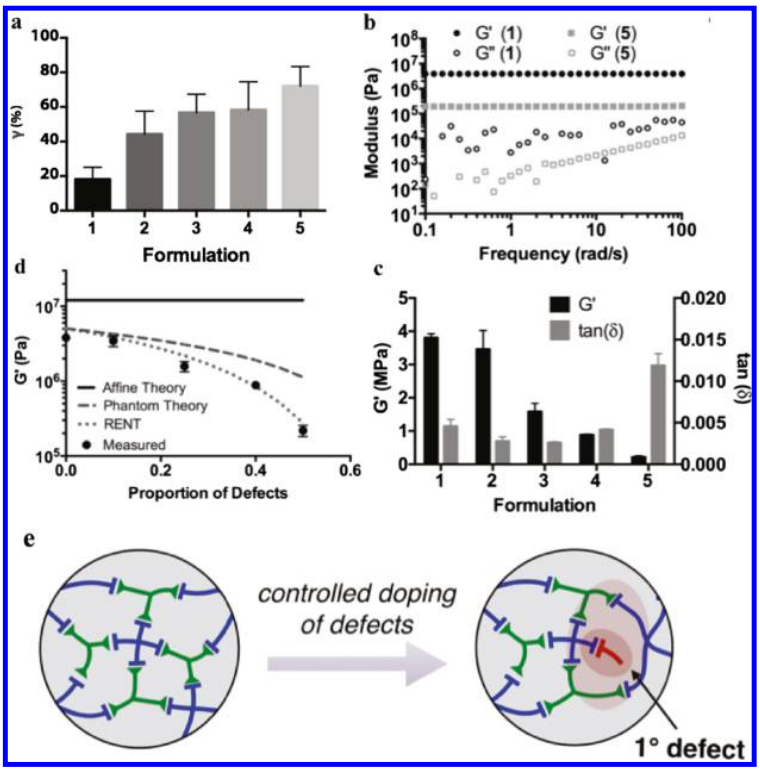

Figure 2. Mechanical characterizations of elastomers using oscillatory shear rheometry. (a) Shear−strain at deviation from linear viscoelastic behavior taken from an oscillatory strain sweep (ω = 10 rad/s, 25 °C; n = 3; data presented as mean ± SD). (b) Frequency-dependent oscillatory shear rheology of samples **1** and **5** (γ = 0.1%, 25 °C). (c) Shear storage modulus (G') and tan(δ) values for various samples (ω = 10 rad/s, γ = 0.1%, 25 °C; n = 3; data presented as mean ± SD). (d) Overlay of measured and predicted G' values, whereby RENT exhibits clear improvement over affine and phantom theories. (e) Doping of primary defects through the addition of a monovalent species can be used to precisely tune the mechanical behavior. The mechanical impact of these defects is propagated beyond the defect itself (indicated by a red halo).

postfabrication, potentially facilitating the design and engineering of materials for bottom-up processing.

Although these samples exhibit virtually identical chemistry, the mechanical behavior was expected to change dramatically on account of the presence of primary defects within the network structure. DSC measurements indicated that the glass transition temperature (T_g) for all samples was low (below −10 °C), thus placing them squarely within the rubbery regime (Figure S4). The T_g was observed to decrease with increasing density of primary defects (Table 1), indicating that the presence of these defects increases the mobility of polymer chains within each elastomer. Moreover, the mechanical properties, as characterized with an oscillatory strain amplitude sweep, vary significantly on account of an increase in primary defects. Strain−amplitude oscillatory measurements indicated a broad linear viscoelastic regime with increasing yield strains arising from the presence of more primary defects (Figure 2a). Frequency-sweep oscillatory rheometry showed that the shear storage modulus (G') dominates over the loss modulus (G'') across all observed frequencies for all formulations (Figures 2b, S5, and S6). Although a G' value of ∼3.81 MPa was observed for sample **1**, which had no primary defects, the G' decreased with increasing concentration of primary defects through greater incorporation of **B1**. Interestingly, the loss tangent, tan(δ) (G''/G'; a measure of the network elasticity), is unaffected by the formulation below a critical concentration of network defects (Figure 2c). To ensure that these tests were conducted in the region of the rubbery plateau, similar rheological measurements were performed at T_g + 40 °C for each sample, yielding similar values of G' and an identical trend in loss tangent (Figure S7). The major deviation of values was found only between the loss tangent of formulation **5** at 25 °C and at −10 °C, arising from a larger G''. This likely arises from the condensation of water on the top rheological plate below 0 °C.

In the present work, RENT is adapted to model the mechanical properties of thiol−ene elastomers with primary defects introduced through the incorporation of **B1** in the absence of loops. We include a 5% molar excess of **A4** end-group alkene functionality to promote reactivity and ensure the thiol groups react to completion. At high concentrations of the reactive groups used in these studies, negligible primary or secondary loops are formed.[28] Moreover, the ratio of thiol functionalities to alkene functionalities remains the same across all formulations; thus, when one unit of **B3** is removed, three **B1** units are doped into the network. Therefore, while the functionality is changing, the elastic effect of **B1** propagates throughout the network, as that dead link would have otherwise been elastically effective. The last term in eq 1 represents the termination of a cross-link that would have otherwise been contributing to the network if not for the introduction of **B1**. Thus, mechanically analogous to a primary loop, the presence of **B1** defects hinders the elastic effectiveness of the network in its immediate vicinity, as the effects of the defects will propagate throughout the network. The distance away from the defect site is denoted by m, where m = 0 is the defect itself

DOI: 10.1021/acsami.7b14376
ACS Appl. Mater. Interfaces 2017, 9, 42217−42224

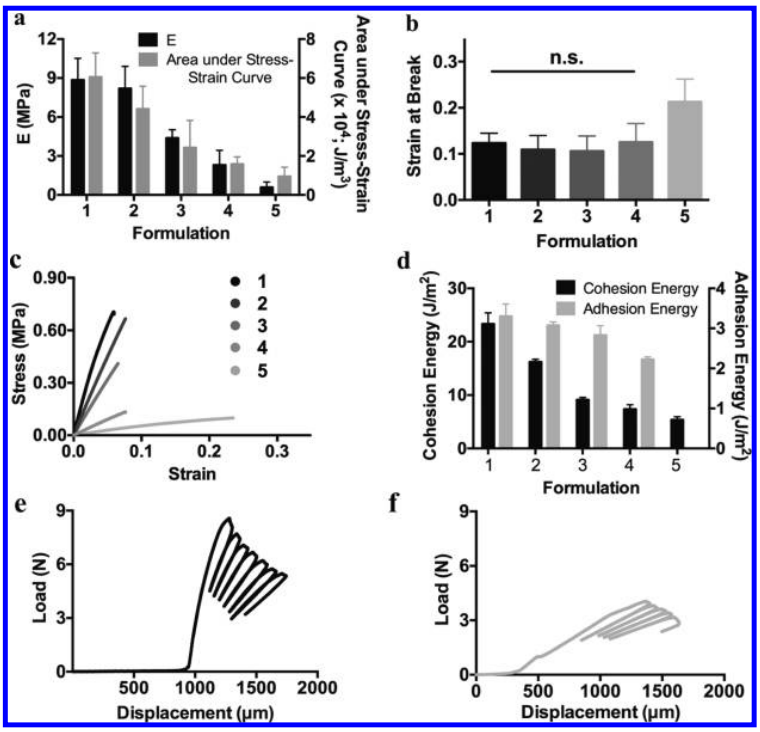

Figure 3. Mechanical characterization of thiol−ene formulations using tensile and DCB measurements. (a) Young's modulus calculated from stress−strain curves, plotted with the modulus of toughness characterized as the area under stress−strain curves (n = 5; data presented as mean ± SD). (b) Strain at break of materials. Statistical analysis across all samples in comparison to 5 yields $p \leq 0.01$ (n = 5; data presented as mean ± SD). (c) Representative stress−strain plots of **1**−**5**. (d) Cohesion and adhesion energies of materials through DCB tests. Statistical analysis of cohesion energies yields $p \leq 0.0001$ for all samples when compared to **5**. The statistical analysis of adhesion energies across all samples in comparison to **4** yields $p \leq 0.001$ ($n \geq 6$; data presented as mean ± SD). (e) Representative DCB graph of **1**, resulting in cohesive delamination. (f) Representative DCB graph of **5**, resulting in cohesive delamination.

and m = 1 is a single network step from the defect site. The RENT model accounts for the linearly additive effects of these defects; here, we include the effects from m =0 to m = 1:

$$G' = \frac{f-2}{f}kT\sum_m \nu_m\varepsilon_m = \frac{f-2}{f}kT\left(\nu_{id} + \sum_0^1 \nu_m\varepsilon_m\right)$$
$$= \frac{f-2}{f}kT(\nu_{id} + \nu_0\varepsilon_0 + \nu_1\varepsilon_1) \quad (1)$$

where f represents the average functionality of the cross-linking nodes as described by eq 2, kT is the thermal energy of the system, ε_m represents the elastic effectiveness of each moiety as described by eq 3, ν is the number density of chains, ν_{id} is the ideal chain density of the polymer, and ν_m is the actual density of each strand in the polymer network at a given value of m, as described by eq 4.

$$f_{avg} = \frac{\sum N_x f_x}{\sum N_x} \quad (2)$$

$$\varepsilon_0 = 0 \text{ and } \varepsilon_1 = 1 - \frac{2}{(f-2)(f-1)} \quad (3)$$

$$\nu_0 = \frac{\nu}{f}N_d \text{ and } \nu_1 = (f-2)\nu_0 \text{ and } \nu_{id} = (1-N_d)\nu \quad (4)$$

Here, N_d represents the proportion of defective links introduced by the incorporation of monovalent thiols, and for each monomer x, N_x represents the molar loading and f_x represents the functionality. RENT accounting for primary defects with proximity effects from m = 0 to m = 1 is in the nearly perfect alignment with observed G' values (Figure 2d). The incorporation of higher-ordered effects (m > 1) into the model resulted in a significant deviation from the observed values (Figure S8), suggesting that higher-order loops play a small role in affecting the elastic modulus.

Although higher-order loops may further reduce the modulus in many other instances, their effect decreases rapidly farther from the defect[21] and can be excluded from the modified theory. Additionally, entanglements may play a role in determining the material properties. Yet in the present system, the low molecular weights of the molecules in the studied bulk-state elastomer are likely to be well below the critical molecular weight regime, and low chain length will lead to a decrease in the interpenetration of chains.[38] Similar polymers, such as PMMA or poly(lactic) acid, have high entanglement molecular weights of 13[39] and 9 kDa,[40] respectively, emphasizing that our low-molecular-weight monomers will be below the critical molecular weight for entanglement. Thus, the alignment of the modified RENT model with the experimental results indicates that other contributory factors to G', such as entanglements, can be neglected and that this modified RENT model is able to successfully predict G' with these considerations. The approach described above allows for the precise introduction of network defects, yielding a simple method for studying their mechanical impact as well as the opportunity to engineer novel network materials with predictable mechanical behavior.

DOI: 10.1021/acsami.7b14376
ACS Appl. Mater. Interfaces 2017, 9, 42217−42224

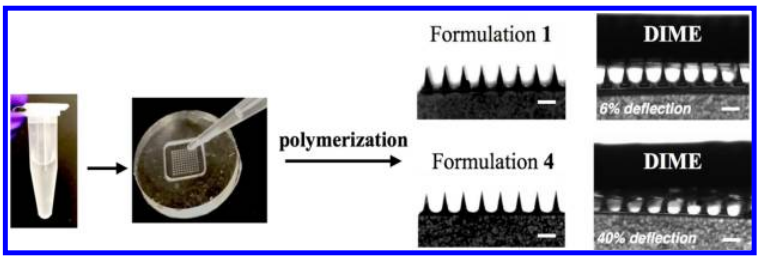

Figure 4. Prepolymer solution can be pipetted into a mold and photopolymerized in situ to form microneedle arrays with similar chemical properties but different mechanical properties, whereby postdeformation under a load (a dime) is highly formulation-dependent (top: **1** and bottom: **4**; scale bar = 650 μm).

To further understand the impact of primary defects on the mechanical properties of the elastomers described above, tensile testing was performed. Young's modulus (E) and the area under the stress−strain curve generated in uniaxial extension decreased notably with the increasing concentration of primary defects, consistent with the observed decrease in T_g and storage modulus (Figure 3a). Interestingly, although samples **1**−**4** exhibited a similar strain at break of ∼10%, sample **5** exhibited a strain at break of over 20% (Figures 3b, 3c). There is an apparent critical concentration of primary defects, leading to a change in strain at break which mimics the observed critical value for the increase in tan(δ) observed in the shear rheological experiments described above (Figure 2c). Below this critical concentration, these elastomers can be modified to modulate the elastic modulus on an order of magnitude while maintaining an unaltered strain at break and tan(δ).

The fracture energy of these materials was then determined for both adhesive and cohesive failure. The critical strain energy release rate, G_c, was measured for all samples using a DCB geometry, which is a well-established method for characterizing thin-film structures and interfaces.[41,42] In these studies, the samples were loaded under displacement control from which a load versus displacement curve was recorded, and G_c was determined according to

$$G_c = \frac{12P_c^2a^2}{B^2E'h^3}\left(1 + 0.64\frac{h}{a}\right)^2 \quad (5)$$

where P_c is the critical load at which the crack growth occurs, a is the crack length, E' is the elastic modulus of the whole structure, and the specimen dimensions are width B and beam thickness h. Note that because the modulus and height of the thin film are less than 1/80th of the modulus and height of the beam used, E' used for the calculation of G_c is that of the beam. Through functionalization and adherence of the materials to beam supports, either adhesive or cohesive failure was induced (Figures 3e, 3f, S9, and S10). The cohesive energy provides an insight into the energy required to break the covalent bonds within the material, whereby a general decline in the cohesive energy was observed with the increasing concentration of primary defects. The binding energy to functionalized glass slides was also examined to specifically investigate the role of internal network mechanics on adhesive energy as the elemental composition was identical across all samples. In these experiments, a small variation in the adhesive energy (<1 J/m^2) was observed between elastomer formulations, in contrast to the changes observed for modulus, T_g, and energy release rate, indicating that surface chemistry is relatively unaffected and is a critical parameter for adhesion. Data were not obtainable for sample **5** on account of its extremely low cohesion energy, which resulted in strictly cohesive failure. This approach to material design utilizing thiol−ene photopolymerization of prepolymer mixtures can allow for the manufacturing of precise structures with identical surface chemistry but with highly tunable mechanical properties (Figure 4). Using a PDMS microneedle mold, we created microneedle arrays of elastomers with different formulations. The mechanical response of the microneedles to loading with a dime differed as expected, whereby needles prepared from formulation **4** exhibited 40% deflection in height, whereas needles prepared from formulation **1** exhibited negligible (6%) deflection.

CONCLUSIONS

In summary, rapid and selective thiol−ene "click" chemistry has proven to be a useful tool for the development of a series of elastomeric polymers with systematic variations in the formulation. Although strategies to tune functionality have been exploited in a variety of applications, a precise relationship between the introduction of primary defects to a comprehensive investigation of its resulting mechanical properties and theory predicting elastic modulus is presented for the first time. The introduction of primary defects into the network structure through the incorporation of a monovalent species does not impact the network or surface chemistry but dramatically impacts the mechanical properties of the materials in a precisely tunable fashion. Further, RENT is adapted to the case of primary defects in the absence of loops, given minimal contribution from entanglements, providing new insights into the mechanism for material strength and failure in cross-linked polymer materials arising from primary network defects. The approach to material design is amenable to a variety of other reaction chemistries (e.g., azide−alkyne reactions[43]) and could lead to new advancements in the development of high-performance materials with precisely defined chemical, physical, and mechanical properties such as stretchable circuits and electronics.[44]

ASSOCIATED CONTENT

Supporting Information

The Supporting Information is available free of charge on the ACS Publications website at DOI: 10.1021/acsami.7b14376.

Complete data sets of material properties for all formulations (storage modulus, transmittance, swelling ratios, DSC results, and DCB results) and further explanations of the calculation and modeling of functionality and shear storage modulus (PDF)

DOI: 10.1021/acsami.7b14376
ACS Appl. Mater. Interfaces 2017, 9, 42217−42224

AUTHOR INFORMATION

Corresponding Author

*E-mail: eappel@stanford.edu.

ORCID

Eric A. Appel: 0000-0002-2301-7126

Author Contributions

The manuscript was written through contributions from all authors. All authors have given approval to the final version of the manuscript.

Notes

The authors declare no competing financial interest.

ACKNOWLEDGMENTS

D.C. is grateful for an award by the Department of Defense, Air Force Office of Scientific Research, National Defense Science and Engineering Graduate (ND-SEG) Fellowship, 32 CFR 168a with government support under FA9550-11-C-0028. A part of this work was performed at the Stanford Nano Shared Facilities (SNSF), supported by the National Science Foundation under award ECCS-1542152.

REFERENCES

(1) Wang, R.; Sing, M. K.; Avery, R. K.; Souza, B. S.; Kim, M.; Olsen, B. D. Classical Challenges in the Physical Chemistry of Polymer Networks and the Design of New Materials. *Acc. Chem. Res.* **2016**, *49*, 2786−2795.

(2) Sundar, V. C.; Zaumseil, J.; Podzorov, V.; Menard, E.; Willett, R. L.; Someya, T.; Gershenson, M. E.; Rogers, J. A. Elastomeric Transistor Stamps: Reversible Probing of Charge Transport in Organic Crystals. *Science* **2004**, *303*, 1644−1646.

(3) Carpi, F.; Bauer, S.; De Rossi, D. Stretching Dielectric Elastomer Performance. *Science* **2010**, *330*, 1759−1761.

(4) Angelopoulos, M. Conducting polymers in microelectronics. *IBM J. Res. Dev.* **2001**, *45*, 57−75.

(5) Städler, B.; Price, A. D.; Zelikin, A. N. A Critical Look at Multilayered Polymer Capsules in Biomedicine: Drug Carriers, Artificial Organelles, and Cell Mimics. *Adv. Funct. Mater.* **2011**, *21*, 14−28.

(6) Ward, M. A.; Georgiou, T. K. Thermoresponsive Polymers for Biomedical Applications. *Polymers* **2011**, *3*, 1215−1242.

(7) Anseth, K. S.; Bowman, C. N.; Brannon-Peppas, L. Mechanical properties of hydrogels and their experimental determination. *Biomaterials* **1996**, *17*, 1647−1657.

(8) Caldwell, A. S.; Campbell, G. T.; Shekiro, K. M. T.; Anseth, K. S. Clickable Microgel Scaffolds as Platforms for 3D Cell Encapsulation. *Adv. Healthcare Mater.* **2017**, *6*, 1700254.

(9) Brochu, P.; Pei, Q. Advances in dielectric elastomers for actuators and artificial muscles. *Macromol. Rapid Commun.* **2010**, *31*, 10−36.

(10) Baughman, R. H. Playing Nature's Game with Artificial Muscles. *Science* **2005**, *308*, 63−65.

(11) Jung, K.; Kim, K. J.; Choi, H. R. A self-sensing dielectric elastomer actuator. *Sens. Actuators, A* **2008**, *143*, 343−351.

(12) Balakrishnan, B.; Jayakrishnan, A. Self-cross-linking biopolymers as injectable in situ forming biodegradable scaffolds. *Biomaterials* **2005**, *26*, 3941−3951.

(13) Jeong, M.-H.; Lee, K.-S.; Lee, J.-S. Cross-Linking Density Effect of Fluorinated Aromatic Polyethers on Transport Properties. *Macromolecules* **2009**, *42*, 1652−1658.

(14) Lee, K. Y.; Rowley, J. A.; Eiselt, P.; Moy, E. M.; Bouhadir, K. H.; Mooney, D. J. Controlling Mechanical and Swelling Properties of Alginate Hydrogels Independently by Cross-Linker Type and Cross-Linking Density. *Macromolecules* **2000**, *33*, 4291−4294.

(15) Oh, K. S.; Oh, J. S.; Choi, H. S.; Bae, Y. C. Effect of Cross-Linking Density on Swelling Behavior of NIPA Gel Particles. *Macromolecules* **1998**, *31*, 7328−7335.

(16) Yu, Y.; Nakano, M.; Shishido, A.; Shiono, T.; Ikeda, T. Effect of Cross-linking Density on Photoinduced Bending Behavior of Oriented Liquid-Crystalline Network Films Containing Azobenzene. *Chem. Mater.* **2004**, *16*, 1637−1643.

(17) Nair, D. P.; Podgórski, M.; Chatani, S.; Gong, T.; Xi, W.; Fenoli, C. R.; Bowman, C. N. The Thiol-Michael Addition Click Reaction: A Powerful and Widely Used Tool in Materials Chemistry. *Chem. Mater.* **2014**, *26*, 724−744.

(18) Cramer, N. B.; Couch, C. L.; Schreck, K. M.; Boulden, J. E.; Wydra, R.; Stansbury, J. W.; Bowman, C. N. Properties of methacrylate-thiol-ene formulations as dental restorative materials. *Dent. Mater.* **2010**, *26*, 799−806.

(19) Mark, J. E. Some Interesting Things about Polysiloxanes. *Acc. Chem. Res.* **2004**, *37*, 946−953.

(20) Mark, J. E. Molecular Aspects of Rubberlike Elasticity. *Acc. Chem. Res.* **1985**, *18*, 202−206.

(21) Zhong, M.; Wang, R.; Kawamoto, K.; Olsen, B. D.; Johnson, J. A. Quantifying the impact of molecular defects on polymer network elasticity. *Science* **2016**, *353*, 1264−1268.

(22) Müllen, K. Molecular defects in organic materials. *Nat. Rev. Mater.* **2016**, *1*, 1−2.

(23) Wang, R.; Johnson, J. A.; Olsen, B. D. Odd−Even Effect of Junction Functionality on the Topology and Elasticity of Polymer Networks. *Macromolecules* **2017**, *50*, 2556−2564.

(24) Zhou, H.; Woo, J.; Cok, A. M.; Wang, M.; Olsen, B. D.; Johnson, J. A. Counting primary loops in polymer gels. *Proc. Natl. Acad. Sci. U.S.A.* **2012**, *109*, 19119−19124.

(25) Andrady, A. L.; Llorente, M. A.; Sharaf, M. A.; Rahalkar, R. R.; Mark, J. E.; Sullivan, J. L.; Yu, C. U.; Falender, J. R. Model Networks of End-Linked Polydimethylsiloxane Chains. XII. Dependence of Ultimate Properties on Dangling-Chain Irregularities. *J. Appl. Polym. Sci.* **1981**, *26*, 1829−1836.

(26) Andrady, A. L.; Llorente, M. A.; Mark, J. E. Effects of dangling chains on some dynamic mechanical properties of model poly-(dimethylsiloxane) networks. *Polym. Bull.* **1992**, *28*, 103−108.

(27) Gu, Y.; Kawamoto, K.; Zhong, M.; Chen, M.; Hore, M. J. A.; Jordan, A. M.; Korley, L. T. J.; Olsen, B. D.; Johnson, J. A. Semibatch monomer addition as a general method to tune and enhance the mechanics of polymer networks via loop-defect control. *Proc. Natl. Acad. Sci. U.S.A.* **2017**, *114*, 4875−4880.

(28) Kawamoto, K.; Zhong, M.; Wang, R.; Olsen, B. D.; Johnson, J. A. Loops versus Branch Functionality in Model Click Hydrogels. *Macromolecules* **2015**, *48*, 8980−8988.

(29) Kade, M. J.; Burke, D. J.; Hawker, C. J. The power of thiol-ene chemistry. *J. Polym. Sci., Part A: Polym. Chem.* **2010**, *48*, 743−750.

(30) Nair, D. P.; Cramer, N. B.; Scott, T. F.; Bowman, C. N.; Shandas, R. Photopolymerized Thiol-Ene Systems as Shape Memory Polymers. *Polymer* **2010**, *51*, 4383−4389.

(31) Blasco, E.; Wegener, M.; Barner-Kowollik, C. Photochemically Driven Polymeric Network Formation: Synthesis and Applications. *Adv. Mater.* **2017**, *29*, 1604005.

(32) Andrzejewska, E. Photopolymerization kinetics of multifunctional monomers. *Prog. Polym. Sci.* **2001**, *26*, 605−665.

(33) Hoyle, C. E.; Lowe, A. B.; Bowman, C. N. Thiol-click chemistry: a multifaceted toolbox for small molecule and polymer synthesis. *Chem. Soc. Rev.* **2010**, *39*, 1355−1387.

(34) Hoyle, C. E.; Bowman, C. N. Thiol-ene click chemistry. *Angew. Chem., Int. Ed.* **2010**, *49*, 1540−1573.

(35) Lu, H.; Carioscia, J. A.; Stansbury, J. W.; Bowman, C. N. Investigations of step-growth thiol-ene polymerizations for novel dental restoratives. *Dent. Mater.* **2005**, *21*, 1129−1136.

(36) Gupta, N.; Lin, B. F.; Campos, L. M.; Dimitriou, M. D.; Hikita, S. T.; Treat, N. D.; Tirrell, M. V.; Clegg, D. O.; Kramer, E. J.; Hawker, C. J. A versatile approach to high-throughput microarrays using thiol-ene chemistry. *Nat. Chem.* **2010**, *2*, 138−145.

(37) Campos, L. M.; Meinel, I.; Guino, R. G.; Schierhorn, M.; Gupta, N.; Stucky, G. D.; Hawker, C. J. Highly Versatile and Robust Materials for Soft Imprint Lithography Based on Thiol-ene Click Chemistry. *Adv. Mater.* **2008**, *20*, 3728−3733.

DOI: 10.1021/acsami.7b14376
ACS Appl. Mater. Interfaces 2017, 9, 42217−42224

(38) Sharaf, M. A.; Mark, J. E. Interpretation of the small-strain moduli of model networks of polydimethylsiloxane. *Polymer* **1994**, *35*, 740−751.
(39) Prentice, P. Influence of molecular weight on the fracture of poly(methyl methacrylate) (PMMA). *Polymer* **1983**, *24*, 344−350.
(40) Palade, L.-I.; Lehermeier, H. J.; Dorgan, J. R. Melt Rheology of High L-Content Poly(lactic acid). *Macromolecules* **2001**, *34*, 1384−1390.
(41) Snodgrass, J. M.; Pantelidis, D.; Jenkins, M. L.; Bravman, J. C.; Dauskardt, R. H. Subcritical debonding of polymer/silica interfaces under monotonic and cyclic loading. *Acta Mater.* **2002**, *50*, 2395−2411.
(42) Sharratt, B. M.; Wang, L. C.; Dauskardt, R. H. Anomalous debonding behavior of a polymer/inorganic interface. *Acta Mater.* **2007**, *55*, 3601−3609.
(43) Lowe, A. B.; Hoyle, C. E.; Bowman, C. N. Thiol-yne click chemistry: A powerful and versatile methodology for materials synthesis. *J. Mater. Chem.* **2010**, *20*, 4745−4750.
(44) Liu, X.; Tang, T.-C.; Tham, E.; Yuk, H.; Lin, S.; Lu, T. K.; Zhao, X. Stretchable living materials and devices with hydrogel-elastomer hybrids hosting programmed cells. *Proc. Natl. Acad. Sci. U.S.A.* **2017**, *114*, 2200−2205.

DOI: 10.1021/acsami.7b14376
ACS Appl. Mater. Interfaces 2017, 9, 42217−42224